https://doi.org/10.7494/geom.2025.19.3.31

Hari Soekarno[1], Bono Pranoto[2], Andini Restiana[3], Agustya Adi Martha[4], Tio Azhar Prakoso Setiadi[5], Nurul Hudayat[6], Achmad Fachrudin Rais[7], Yatin Suwarno[8], Turmudi[9], Bayu Sutejo[10]

Identifying Geological Fault Structures Using GGMplus Satellite Data and Derivative Methods to Characterize Mount Endut Geothermal Systems via 3D-Inversion Gravity Modeling

Abstract: The geological map shows that the Mount Endut area possesses a geothermal system, which is suggested by the presence of geothermal surface manifestations: the Cikawah and Handeleum hot springs. The existence of a subsurface geological fault structure along the manifestations creates good permeability for the geothermal reservoir. The purpose of this study was to utilize Global Gravity Model plus (GGMplus) gravity satellite data to prove the existence of a geological fault structure around the manifestation area with the first horizontal derivative (FHD) and second vertical derivative (SVD) methods; then, we developed a conceptual model of the geothermal system from the 3D-inversion gravity method. Results show a cap suspected of being clay, with a density of 2.52–2.58 g/cm^3 at depth of 0–1250 m. The reservoir layer was suspected to be lava rock with a density of 2.60–2.66 g/cm^3 at a depth of 1500–3000 m; also, the heat source layer was suspected to be an igneous intrusion with a density of 2.70–2.72 g/cm^3 at depth of 1750–3000 m.

Keywords: GGMplus, derivative method, geological fault structure, first horizontal derivative (FHD) method, second vertical derivative (SVD) method

Received: June 9, 2023; accepted: April 24, 2025

[1] National Research and Innovation Agency (BRIN), Research Center for Limnology and Water Resources, Bogor, Indonesia, email: hari053@brin.go.id
[2] BRIN, Research Center for Limnology and Water Resources, Bogor, Indonesia, email: bono001@brin.go.id (corresponding author), https://orcid.org/0000-0002-2772-6528
[3] Syarif Hidayatullah Islamic University, Faculty of Science and Technology, Jakarta, Indonesia, email: andinirestianaa@gmail.com
[4] BRIN, Research Center for Limnology and Water Resources, Bogor, Indonesia, email: agus176@brin.go.id, https://orcid.org/0000-0003-3630-093X
[5] BRIN, Research Center for Limnology and Water Resources, Bogor, Indonesia, email: tioa001@brin.go.id, https://orcid.org/0000-0002-2429-6147
[6] BRIN, Research Center for Limnology and Water Resources, Bogor, Indonesia, email: nuru047@brin.go.id, https://orcid.org/0000-0003-2251-2843
[7] BRIN, Research Center for Limnology and Water Resources, Bogor, Indonesia, email: achm050@brin.go.id, https://orcid.org/0000-0002-4125-4387
[8] BRIN, Research Center for Limnology and Water Resources, Bogor, Indonesia, email: yati005@brin.go.id, https://orcid.org/0000-0002-2963-7182
[9] BRIN, Research Center for Limnology and Water Resources, Bogor, Indonesia, email: turm001@brin.go.id, https://orcid.org/0009-0006-9773-3287
[10] BRIN, Research Center for Limnology and Water Resources, Bogor, Indonesia, email: bayu002@brin.go.id, https://orcid.org/0009-0002-1543-0831

1. Introduction

Mount Endut is located in Lebak Regency, Banten Province; the area was indicated as an area with geothermal potential after the discovery of geothermal manifestations in hot springs [1, 2]. For this reason, a preliminary study of the area's geothermal system is needed before geothermal exploitation. The existence of a geothermal system can be obtained through geological and geophysical data analysis. Geological data serves as an illustration of the conditions of potential geothermal areas [3], and geophysical data helps to determine the subsurface conditions (such as the geological structures that are used as fluid-control pathways in geothermal systems) with the physical mapping of various geological components below the surface [2, 4–6].

Recent advances in gravity-data collection have significantly improved the resolution and accuracy of subsurface imaging. One of the most promising tools in this regard is Global Gravity Model Plus (GGMplus), which was developed through a collaboration between Curtin University (Perth) and the Technical University of Munich (TUM) [7]. GGMplus is a gravity-modeling technique that utilizes gravity data that is obtained from satellite measurements in order to analyze and interpret various geological phenomena. GGMplus data has a high spatial resolution, with a grid spacing of approximately 200 m [8]; this allows for the detailed mapping and analysis of gravity disturbances and anomalies [9–16].

The gravity data from GGMplus can be analyzed using derivative methods such as the first horizontal derivative (FHD) [17] and the second vertical derivative (SVD) [18]. These methods have been shown to effectively delineate fault boundaries and provide insight into subsurface structural configurations [6, 19]. Additionally, the modern 3D-inversion modeling of gravity data has emerged as a robust method for constructing conceptual models of geothermal systems, further aiding in the assessments of subsurface conditions [12, 13].

This research conducted a fault analysis that controlled the manifestation of Cikawah and Handeleum and carried out 3D modeling using the gravity method on satellite data that originated from GGMplus.

2. Materials and Method

The gravity method is widely used to identify the presence of geological faults [20] as well as the rocks that make up a geothermal system. However, identifying the presence of fault structures requires supplementary techniques to offer a clearer representation, so further methods are needed in order to provide a clear picture; namely, by using the FHD and SVD methods to further refine fault-boundary detection.

This research was conducted to prove the existence of a fault that controlled the manifestation of Cikawah and Handeleum and carried out 3D-inversion modeling

using the gravity method on data that originated from GGMplus. Several scientific and engineering applications require high-resolution and largely complete gravity knowledge; this is now available through GGMplus gravity data [7]. A research flowchart is shown in Figure 1.

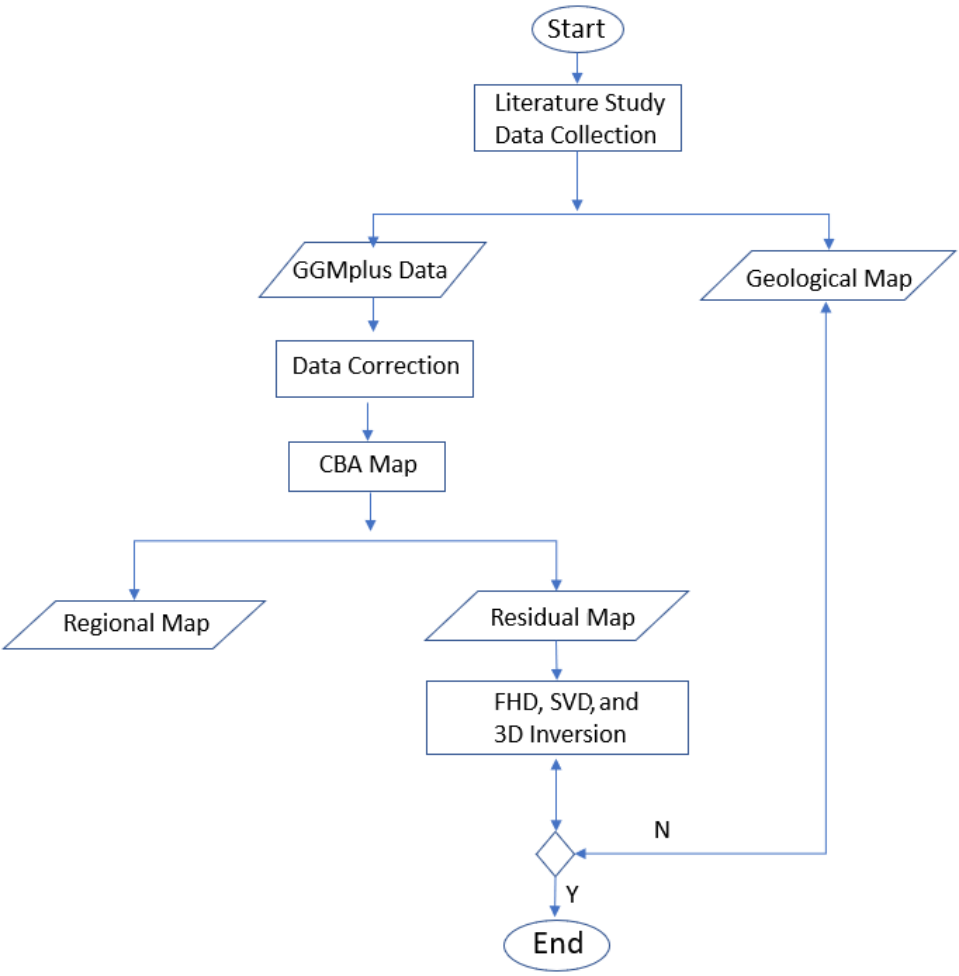

Fig. 1. Research flowchart

2.1. Geological Setting

The morphology of the Mount Endut is classified into four units: complex cone (35%), volcanic cone (25%), weakly undulating hill (32%), and flat plain (8%).

The stratigraphy of the Mount Endut area consists of 16 rock units that range in age from Tertiary to Quaternary. The sequence of these units from oldest to youngest

is as follows: the Baduy sediment member unit (Tmd), the Bojongmanik sediment member unit (Tmb), Andesitic intrusion (Ta), Pre-Endut volcanic rock (Tlpe), Mt. Kendeng lava breccia (Tbr), Mt. Pilangranal lava (Tlr), Diorite (Td), Granodiorite (Tgr), Mt. Pilar breccia lava (Qbp), Mt. Pilar lava (Qlp), Endut lava 1 (Qle1), Endut Pyroclastic Flow (Qae), Endut lava 2 (Qle2), Endut lava breccia (Qbe), Endut Lava 3 (Qle3), and Alluvium (Qal). The geological structure of the Mount Endut area is manifested by the presence of hill alignments (lineaments), volcanic cones, topographic alignments, triangular facets, fault scarps, joints, rock offsets, and fault mirrors (slickensides) as well as the emergence of geothermal manifestations and altered rocks (Fig. 2). In several areas, Mount Endut has limestone facies that generally deposit in marine environments. Based on the geological map of the Leuwidamar Sheet, the limestone facies in the study area are part of the Bojongmanik and Badui Formations and are in the Bogor Physiographic Zone [22]. The geothermal manifestations of Mount Endut are in the forms of hot springs that appear at several manifestation locations in the Cikawah and Handeuleum areas (located at the western foot of Mount Endut) [23].

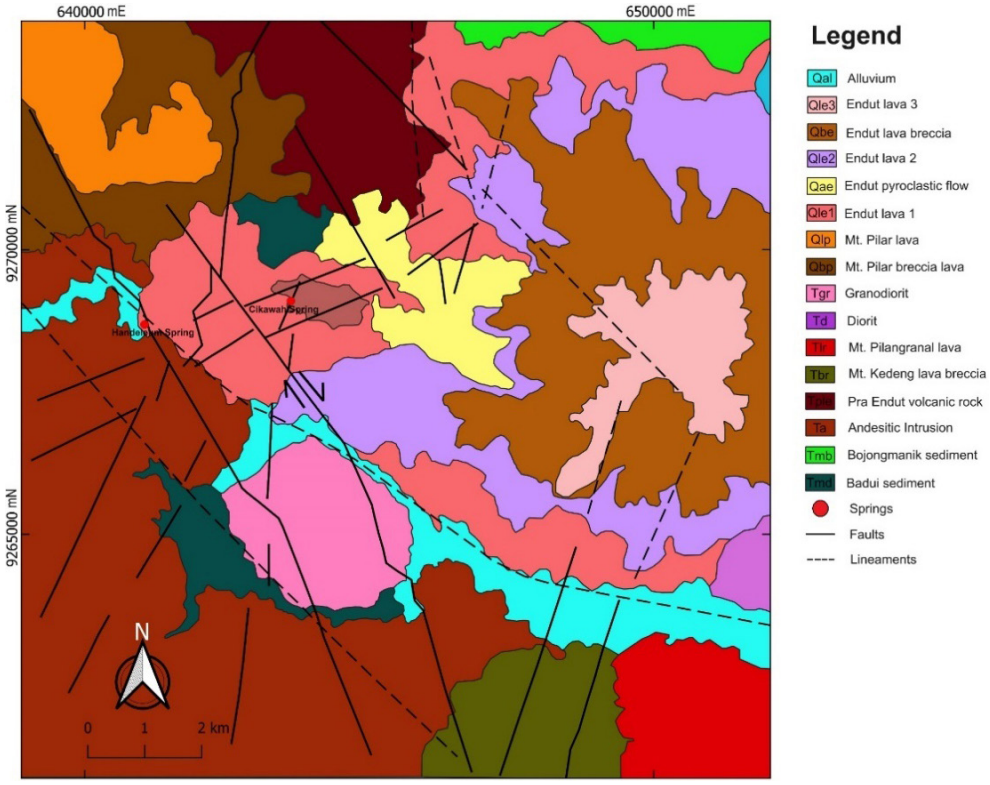

Fig. 2. Geological map of Mount Endut
Source: [21]

2.2. GGMplus Data

GGMplus resulted from a Curtin University (Perth, Western Australia) research initiative and the Technical University of Munich, Germany. GGMplus is a gravity model that was derived from space satellites and a combined solution of the three main constituents of satellite gravity; namely, GOCE/GRACE (with a spatial scale of 10,000–100 km), EGM2008 (100–10 km), and gravity topography (from 10 km to 250 m). GGMplus data provides high-resolution images of all continents, coastal zones, and islands within the latitudes of ±60° [7] by integrating data from 14 new satellite and terrestrial gravity sources with topographical information and employing extensive parallel-computing methods to provide local details at an approximate spatial resolution of 200 m.

The GOCE (Gravity field and steady-state Ocean Circulation Explorer) satellite is a gravity-meter satellite that aims to determine gravitational fields in the forms of geoids and gravitational anomalies that have accuracies of 1 centimeter for geoid height, 1 mGal for gravity anomalies, and 100 km for grid spacing on the surface. The GOCE data provides a unique model in the gravitational field and the terms of the representation of the equipotential area that the geoid represents. Meanwhile, the GRACE (Gravity Recovery and Climate Experiment) satellites (namely, gravity-meter satellites) detect changes in the gravitational field by monitoring changes in the distance that occurs between them in their orbits (with a distance of 220 km between the two satellites). These satellites are connected to the K-band microwave link to calculate the differences in distance. These satellites are equipped with a star camera, an accelerometer, and GPS. The GRACE satellites have provided reasonably accurate information from a model of the Earth's gravitational field for five years [24].

ERTM (Earth Residual Terrain Modelled-gravity field) is a short-scale Earth gravity field that is obtained by advanced high-resolution gravity modeling using SRTM (Shuttle Radar Topography Mission) global topography. ERTM has a spatial scale with a spherical harmonic coefficient of up to 2160 degrees, which is used in making GGMplus gravity maps on short scales from 10 km to 250 m [25, 26].

In selecting GGMplus for the gravity-data analysis in this study, several additional factors beyond those that were mentioned before warranted consideration. First, GGMplus offers a global gravity-field model that is continuously updated, thus ensuring that the data reflects the most current understanding of our gravitational variations. This is particularly important in geothermal studies, where subtle changes in gravity can indicate the presence of geothermal reservoirs or fault lines [27, 28]. Furthermore, GGMplus incorporates a multi-resolution approach, thus allowing for the integration of both high-resolution local data and broader regional data sets [29]. This capability enables researchers to analyze gravity anomalies at various scales, thus facilitating a more comprehensive understanding of the geological context.

Additionally, GGMplus provides access to a wealth of ancillary data, including topographic and geological information (which can be crucial for interpreting gravity anomalies of surface features) [6, 30]. The software also supports advanced filtering techniques that can enhance the clarity of the gravity data by minimizing noise and artifacts, thus improving the accuracy of subsequent analyses [31]. Moreover, the user-friendly interface of GGMplus allows for efficient data manipulation and visualization, making it easier for researchers to communicate their findings and engage interactively with the data [32]. Last, the strong community support and extensive documentation that are associated with GGMplus foster a collaborative environment for researchers, thus enabling them to share insights and methodologies that can enhance the overall quality of geophysical research. These factors collectively underscore the rationale for choosing GGMplus as a pivotal tool in the investigation of the geothermal systems at Mount Endut.

Traditional gravity methods, which typically entail the collection of gravity data from ground stations, can be labor-intensive and have limited spatial coverage. In contrast, GGMplus integrates satellite data, thus providing a more comprehensive view of gravitational anomalies across vast areas without the need for extensive ground surveys. This capability is crucial for the preliminary mapping and understanding of geological features before conducting more-invasive ground-based investigations [33, 34]. For example, GGMplus data has been successfully utilized in studies that have identified geothermal systems and fault structures, thus demonstrating its effectiveness in enhancing traditional methodologies [27, 35].

2.3. Data Corrections

The data that was obtained when downloading from GGMplus was still in the form of gravity disturbances and not yet in the form of a free-air gravity anomaly (where the GGMplus data is only corrected up to latitude correction). Therefore, the GGMplus data still needed some corrections; these will be outlined in the following sections.

Free-Air Correction

Free-air correction was carried out due to the influence of the altitude variations on the Earth's gravitational field. Gravity measurements have different results at certain heights and at mean sea level; any changes in the height will have a changing gravity value as compared to the mean sea level [36]. Each observation point was not always at the mean sea level; so, a free-air correction was needed using following formula [37]:

$$FAC = 0.3086 \cdot h \tag{1}$$

where:

FAC – free-air correction [mGal],

h – altitude or elevation value that is obtained from the geoid.

Free-Air-Anomaly Correction

Free-air-anomaly correction has an influence that originates from a gravity disturbance (δg). To get the free-air anomaly at a specific position, it is necessary to correct any free-air anomalies.

The following is the formula for finding free-air-anomaly values [37]:

$$FAA = \left(0.3086 \cdot h\right) - \delta g = FAC - \delta g \tag{2}$$

where:

FAA – free-air anomaly [mGal],
FAC – free-air correction [mGal],
δg – gravity disturbance value from GGMplus data [mGal],
h – altitude or elevation value that is obtained from geoid [m].

Terrain Correction

Terrain correction is a correction that is caused by the differences in irregular topographical forms at measurement points, such as mountains, hills, and valleys; this affects the gravity value that is obtained. For this reason, terrain corrections are carried out in order to obtain a value that is close to the rock configuration [33].

Terrain corrections can be obtained using the Hammer chart method or DEM (digital elevation model) maps. The calculations of terrain corrections in this study used Geosoft software by entering the data in the form of coordinates (X, Y) and DEM.

The following is the equation for field corrections [38]:

$$TC = G\rho\theta\left[(r_2 - r_1) + \sqrt{r_1^2 + z^2} - \sqrt{r_2^2 + z^2}\right] \tag{3}$$

where:

TC – field correction [mGal],
G – Newton's gravitational constant [Nm^2/kg^2] ($G = 6.67430 \cdot 10^{-11}$ Nm^2/kg^2),
ρ – rock density [kg/m^3],
θ – angle formed [°],
r_1 – radius of inner circle [m],
r_2 – radius of outer circle [m],
z – altitude/depth of field [m] (an absolute difference between the station elevation and the average elevation ($z = |z_{stations} - z_{average}|$).

This equation estimates the gravitational effect of the terrain in each sector of the Hammer chart; the total terrain corrections are obtained by summing up the contributions from all of the sectors. The average altitude within a single compartment is estimated from the contour lines within this compartment and then subtracted from the station altitude. The difference in altitude (z) is used to calculate the terrain-correction contribution for each compartment. To obtain the total terrain correction, we summed up all of the contributions from the innermost sector to the outermost sector, resulting in the final terrain correction value.

Bouguer Correction

Bouguer correction is a correction that is made to the height by considering the mass of the rock around the point of a measurement. Bouguer correction is different from free-air correction; free-air correction only calculates the effect of the difference in height by ignoring the rock mass so that the higher the measurement station, the smaller the gravity value is (because it is further from the center of the Earth). At the same time, Bouguer correction is a correction that is influenced by altitude, and it calculates the value of the rock density. This correction eliminates the pulls of rock masses at certain heights [33]. The equation for calculating Bouguer corrections is as follows [37]:

$$BC = 0.0419 \cdot \rho \cdot h \tag{4}$$

where:

BC – Bouguer correction [mGal],
ρ – density [g/cm^3],
h – altitude [m].

Simple Bouguer Anomaly Correction

Simple Bouguer anomaly correction is obtained based on a free-air correction and Bouguer correction calculation; gravity is needed for simple Bouguer anomaly calculations and obtaining complete Bouguer anomaly values. The following is a simple Bouguer anomaly formula [39]:

$$SBA = FAA - BC \tag{5}$$

where:

SBA – simple Bouguer anomaly [mGal],
FAA – free-air anomaly [mGal],
BC – Bouguer correction [mGal].

Complete Bouguer Anomaly Correction

Complete Bouguer anomaly (CBA) correction is the sum of the simple Bouguer anomaly and terrain corrections. CBA describes the density conditions below the surface of the study area (which later requires separations between the regional and residual anomalies for further analysis) [39]. The following is the equation for obtaining CBA correction:

$$CBA = SBA + TC \tag{6}$$

where:

CBA – complete Bouguer anomaly [mGal],
SBA – simple Bouguer anomaly [mGal],
TC – terrain correction [mGal].

2.4. Energy Spectrum Analysis

Spectrum analysis is performed to separate regional and residual anomalies so that the estimated depth of an anomaly can be determined. This analysis is done with the Fourier transform, which is used to convert time-domain data into a frequency domain. Systematically, the spectrum value results from the gravitational potential derivative in the horizontal plane. The Fourier transform can be written with the following equation [39]:

$$F[g_z] = 2\pi G\mu e^{|k|(z_0 - z')} \text{ with } z' > z_0 \tag{7}$$

where:

$F[g_z]$ – Fourier transform of gravitational acceleration derivative (vertical component) [s^{-2}],
G – Newton's gravitational constant [Nm^2/kg^2] ($G = 6.67430 \cdot 10^{-11}$ Nm^2/kg^2),
μ – body mass [kg],
z_0 – height of measurement point [m],
z' – anomaly depth [m].

The processing of the energy-analysis data uses Oasis Montaj software to produce a radially averaged power spectrum (RAPS) curve from the Fourier transform process, which is displayed in the logarithmic value of the normalized energy spectrum at each radial frequency value. To carry out a depth analysis with wave number (k) and amplitude (A) values, it can be done to separate the regional and residual anomalies by determining the cutoff area of the existing spectrum analysis [39].

2.5. Bandpass Filters

A gravity anomaly is the sum of the sources of an anomaly under a surface [40]; so, it is necessary to separate the regional anomaly, residual anomaly, and noise. The separation can be done by using the existing filtering method on the gravity data [20]. The filtering method that was used in this study was the bandpass filter method; a bandpass filter is a filter that can remove noise signals from research data so that one can retrieve the desired data. This filter is done by filtering the data within a specific time range between the lower and upper cut-off frequencies [41, 42].

2.6. Derivative Analysis

Derivative analysis is an analysis that is carried out to determine the boundaries of a fault structure that is below a surface by using the first horizontal derivative (FHD) and second vertical derivative (SVD) methods [43].

First Horizontal Derivative (FHD)

FHD is a change in the gravity-anomaly value from one point to the next with a certain distance that has a clear characteristic in the form of a maximum FHD value (peak); therefore, a significant anomaly change indicates the existence of a boundary

of the geological structure of the gravity anomaly. The FHD-value equation is obtained from the following equation [43]:

$$FHD = \sqrt{\left(\frac{\partial g}{\partial x}\right)^2 + \left(\frac{\partial g}{\partial y}\right)^2} \tag{8}$$

where $\partial g/\partial x$ and $\partial g/\partial y$ are the first derivatives of the gravity anomaly in the x and y directions, respectively. In cross-sectional modeling, only the x direction is used; so, this formulation is as follows:

$$FHD = \frac{\partial g}{\partial x} \tag{9a}$$

This equation can be written as follows:

$$\frac{\partial g}{\partial x} = \frac{g_{(i+1)} - g_i}{\Delta x},$$

$$FHD = \frac{g_{(i+1)} - g_i}{\Delta x} \tag{9b}$$

where:

FHD – first horizontal derivative,
g – anomalous value [mGal],
Δx – difference in distance along the track [m].

Second Vertical Derivative (SVD)

SVD is used in interpreting structures that are insufficient in the Bouguer anomaly map to separate the shallow and deep structural effects that result in regional and residual anomalies. A residual anomaly describes a structure that is close to the surface but has not provided specific results; therefore, a second vertical descent is needed for a more specific structural effect [44]. This second vertical descent is a high-pass filter that provides a clear picture of the residual anomalies in shallow structures; therefore, SVD is used to identify the type of down fault or up fault. In the SVD method, the existence of a fault boundary is indicated by an SVD value of zero (or close to zero). The SVD equation is obtained through the horizontal derivative using the Laplace equation for gravity anomalies; namely, the following [18]:

$$\nabla g = 0\,,$$

$$\frac{\partial^2 g}{\partial x^2} + \frac{\partial^2 g}{\partial y^2} + \frac{\partial^2 g}{\partial z^2} = 0 \tag{10}$$

When viewed from the changes in the gravitational field in the horizontal x and vertical z directions, the second derivative in the y direction has a constant value in Equation (10); this becomes the following:

$$\frac{\partial^2 g}{\partial z^2} = -\frac{\partial^2 g}{\partial x^2},$$

$$\frac{\partial^2 g}{\partial z^2} = \frac{\dfrac{g_{(i+1)} - g_{(i)}}{\Delta x} - \left(\dfrac{g_{(i)} - g_{(i-1)}}{\Delta x} \right)}{\Delta x},$$

$$SVD = \frac{g_{(i+1)} + g_{(i-1)} - 2g_i}{\Delta x^2} \tag{11}$$

where:

SVD – second vertical derivative,
g – anomalous value [mGal],
Δx – difference in distance along the track [m].

The fracture type can be identified using the following equation [18]:

$$\left|SVD\right|_{\min} < \left|SVD\right|_{\max} \rightarrow Normal\ Fault,$$

$$\left|SVD\right|_{\min} > \left|SVD\right|_{\max} \rightarrow Up\ Fault,$$

$$\left|SVD\right|_{\min} = \left|SVD\right|_{\max} \rightarrow Flat\ Fault.$$

2.7. 3D-Inversion Modeling

3D-inversion modeling is a backward modeling where the model parameters are generated directly from the obtained data and the adjustment of the results of the calculations and observational data is carried out automatically. It calculates the data using mathematical equations, which are derivatives of physics concepts. Inversion modeling is commonly referred to as data fitting, because searching for model parameters produces a response that matches the observational data [39].

The inversion method relates to model parameters (M) and the amount of data (N) that can determine the classifications of inversion problems and how to solve them. When the number of model parameters is less than the data that is measured in the field ($M < N$), it is called "overdetermined"; so, the solution is to use the best-fit method for the field data. Meanwhile, if the number of parameters that are sought are more than the amount of the data, it is called "underdetermined." If many models match the data, it is called "non-uniqueness." The measurement data lies on the surface, where the amount of data is much smaller than the number of the parameters for which one searches. Therefore, the inversion solution can be obtained by minimizing the model norm.

As a result, the inversion model can be expressed as follows [45]:

$$m = G^T[G^T G + \lambda I]^2 d \tag{12}$$

where:

m – model parameters (density contrast),
G – wavelet matrix,
$G^T G$ – small fraction of the maximum value of the diagonal elements,
λ – damping factor used to reduce overfitting by preventing the model from exactly fitting the observed data,
I – identity matrix (invertible),
d – matrix of anomaly gravity data.

3. Results and Discussion

3.1. Complete Bouguer Anomaly Map

In the obtained CBA map (see Fig. 3), it can be seen that the gravity anomaly values were within a range of 77.8–114.4 mGal.

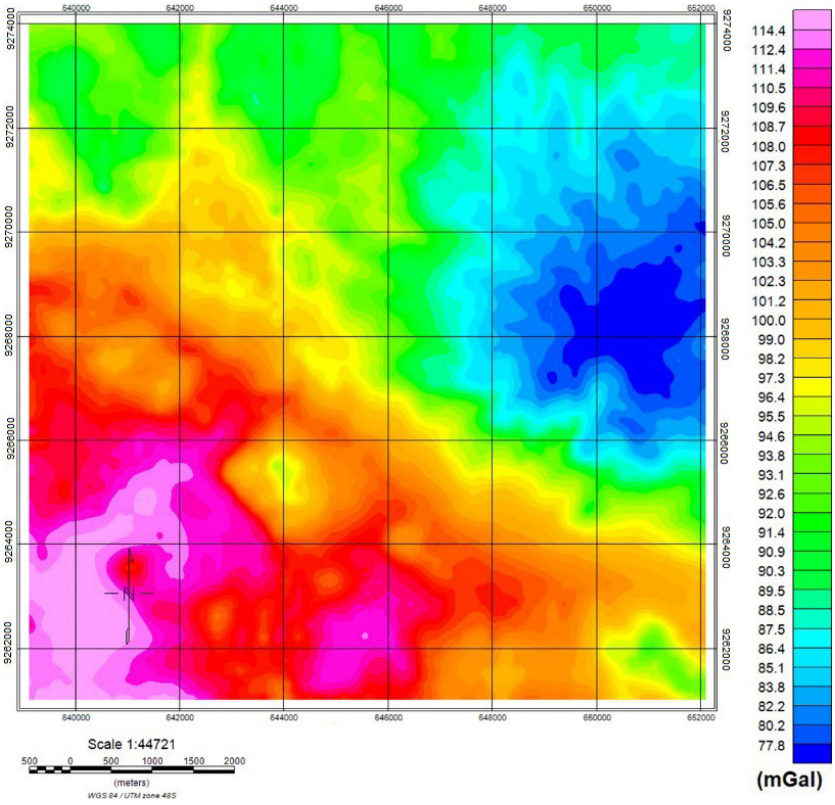

Fig. 3. CBA map of Mount Endut

The distribution of the CBA anomalies described a gravity anomaly that was influenced by the rock-mass-density distribution that was arranged below the surface.

Low anomalies were scattered in the east-northeast part of the study area (marked in blue) and had a range of anomaly values that ranged from 77.8 to 89.5 mGal. Moderate anomalies were scattered in the north and toward the southeast (marked in green), with a range of anomaly values that ranged from 97.3 to 114.4 mGal.

For a comparison, Figure 4 is a CBA map of the results of the gravity measurements in the geothermal prospect area of Mount Endut that were taken by William Jhanesta and Supriyanto Suparno [46].

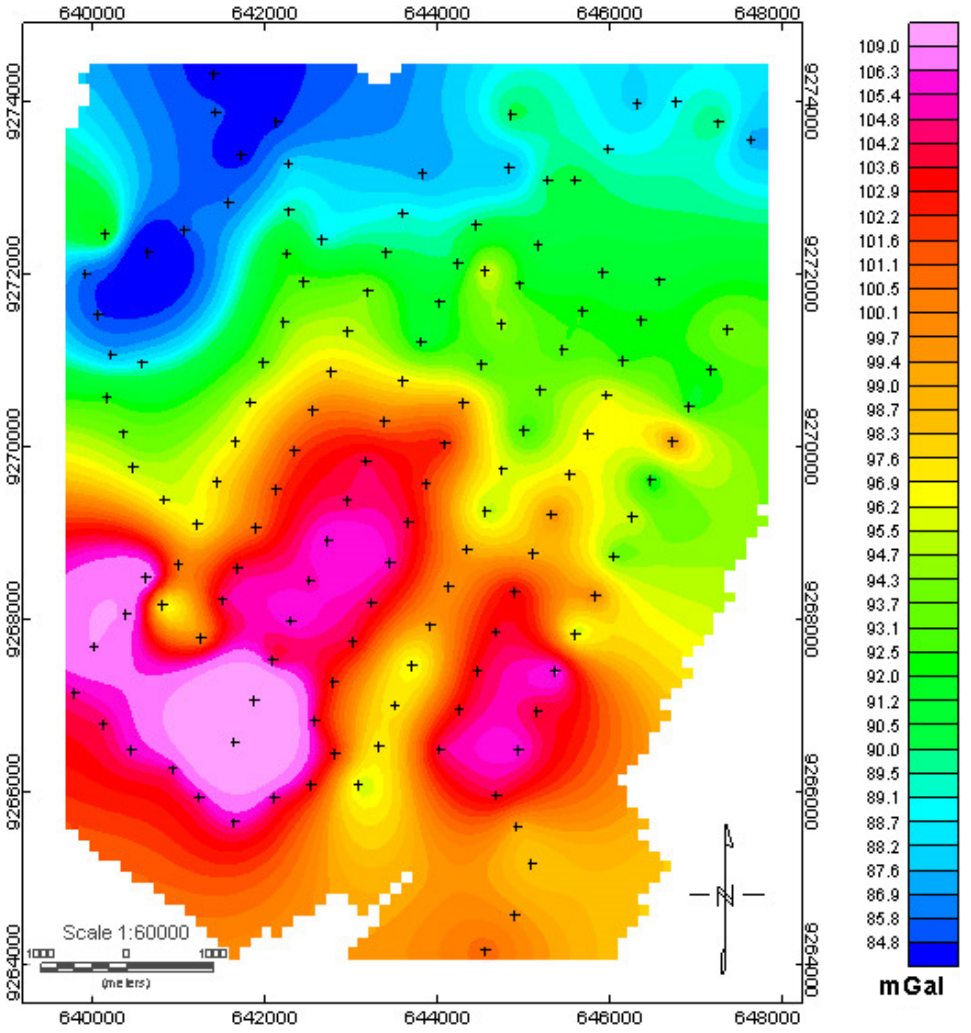

Fig. 4. CBA map from gravity measurements

Source: [46]

Low anomalies (84–89 mGal) are shown in blue, medium anomalies (90–100 mGal) in green, yellow, and orange, and high anomalies (101–109 mGal) in red to purple. Exact values can be found in the color scale.

The comparison results showed that the low-anomaly values from GGMplus were relatively the same as our measurement results, while the upper limits of GGMplus were slightly higher for the results of the medium- and high-anomaly analyses. In addition, the low-anomaly areas of the GGMplus analysis results were below Mount Endut, while the low-anomaly areas shifted westward from Mount Endut in the results of the gravity measurements. One of the advantages of GGMplus is that it could analyze the entire area under Mount Endut as a whole.

The changes in lithology may have caused anomalous contrasts to appear on the CBA map. An interpretation of the CBA map cannot be made yet, because the CBA map is still a combination of regional anomalies, residuals, and noise; so, ambiguity can arise when an interpretation is carried out. Therefore, the regional anomalies, residuals, and noise were separated to eliminate this ambiguity.

3.2. Separation of Regional and Residual Anomalies

The resulting CBA map is a combination of regional anomalies, residuals, and noise values; so, it is necessary to separate these by performing an energy-spectrum analysis on an RAPS curve by delimiting the regional and residual values.

The RAPS curve (Fig. 5) has its main components in the forms of regional anomalies, residual anomalies, and noise. Based on these components, it could be analyzed into a source that was obtained by dividing each component's slope value on the RAPS curve by 4π so that the depth of each element could be identified (shown in Table 1).

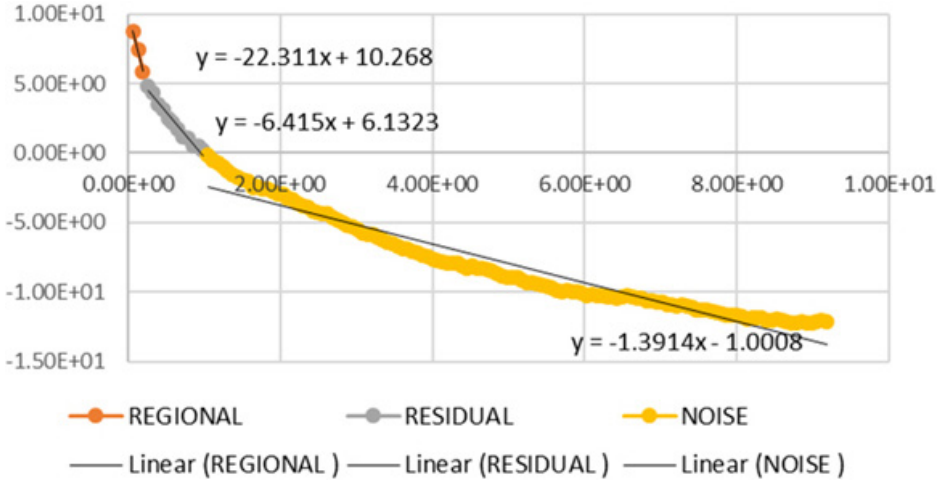

Fig. 5. RAPS curve

Table 1. Ensemble of sources from RAPS curve

Component	Slope [%]	Depth [km]
Regional	22.311	1.77
Residual	6.415	0.51
Noise	1.3914	0.11

3.3. Regional-Anomaly Maps

The regional map (Fig. 6) shows that the resulting regional-anomaly pattern looks similar to the CBA anomaly map; still, the pattern that was obtained is smoother than in the CBA map on the regional anomaly. This was caused by the influence of rock variations that were deep enough where the presence of the lithology in the CBA was relatively more homogeneous.

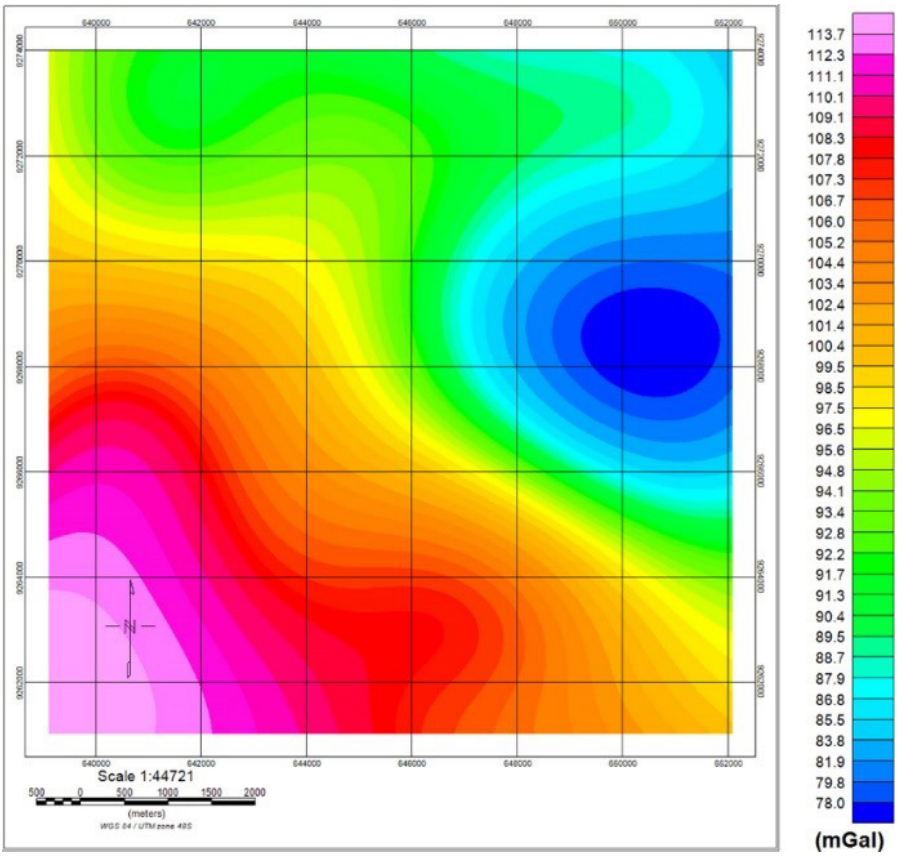

Fig. 6. Regional anomaly map of Mount Endut

The obtained regional-anomaly values ranged from 78.0 to 113.7 mGal, where the low anomalies were scattered in the east-northeast of the study area (with anomaly values that ranged from 78.0 to 88.7 mGal). The moderate anomalies were scattered in the north and toward the southeast, with anomaly values ranging between 89.5 and 95.6 mGal. Meanwhile, the high anomalies were scattered in the southwestern and southern parts, with the anomaly values that ranged from 96.5 to 113.7 mGal.

3.4. Residual-Anomaly Maps

Among the residual anomalies, there were positive and negative anomalies; this can be estimated to be a suspected fault. From the residual map (Fig. 7), 14 suspected fault structures (black lines) are visible in the study area: six faults trended northeast to southwest (F6, F7, F8, F9, F11, and F12), one trended almost north to south (F13), and seven faults trended northwest to southeast (F1, F2, F3, F4, F5, F14, and F10).

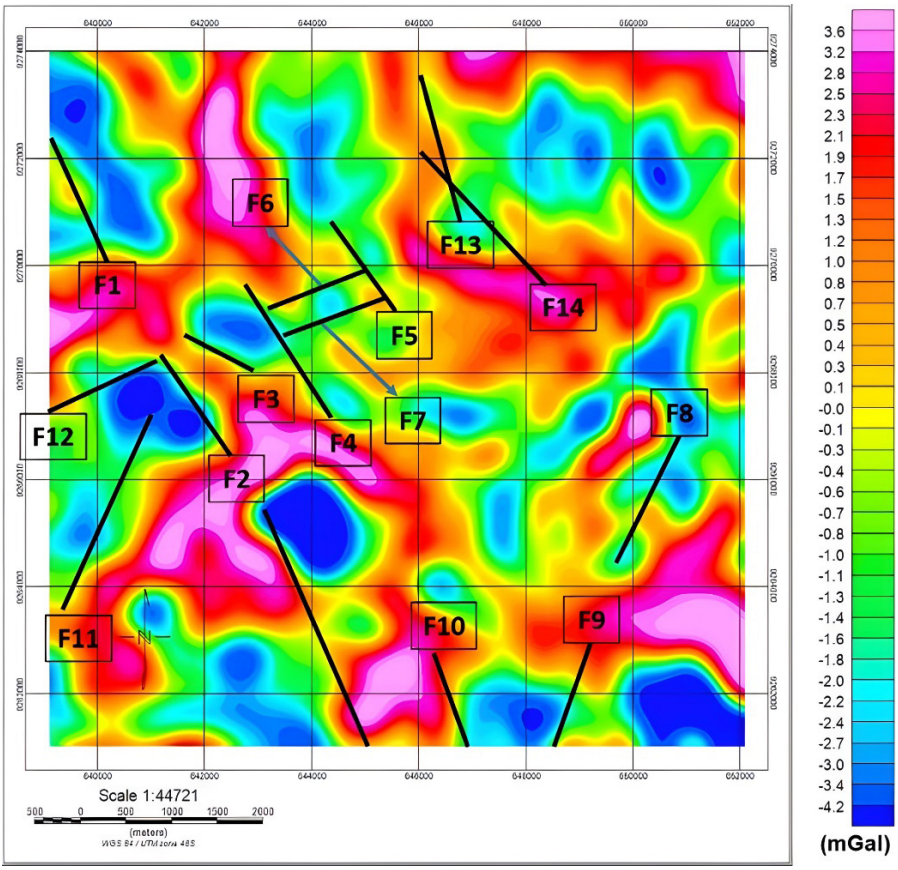

Fig. 7. Residual-anomaly map of Mount Endut

The fault structure that is suspected to be the path for the emergence of the Handeleum hot springs is marked as F3, while the path for the emergence of the Cikawah hot springs is F6. Based on the results of this analysis, there is a compatibility with the faults in the study area (dashed white lines) if the results are overlaid on a geological map; this can be seen in Figure 8.

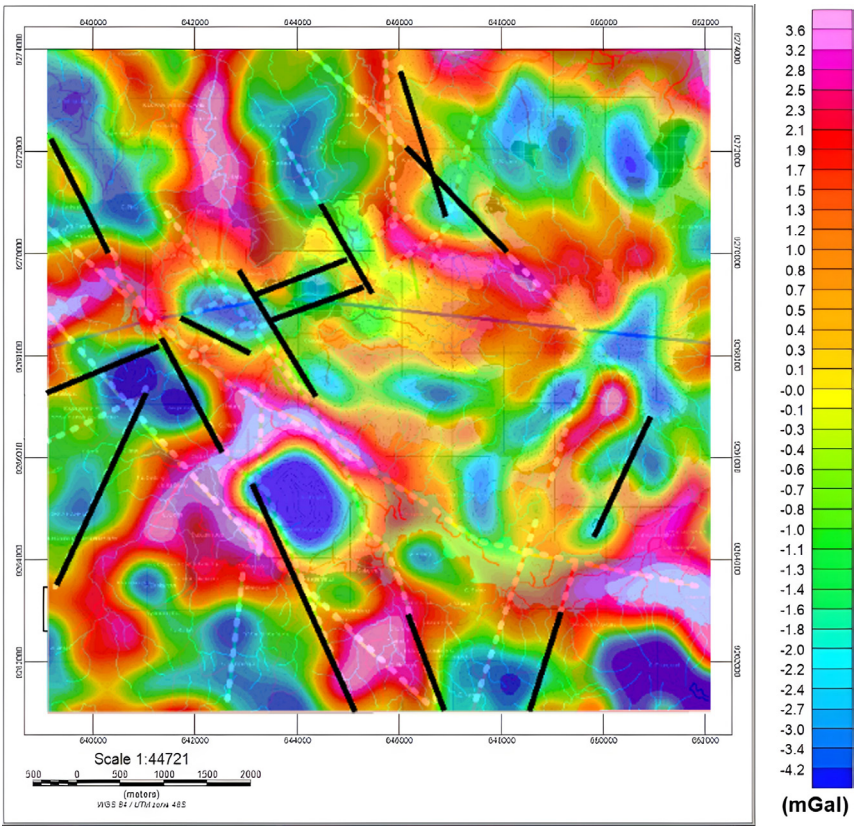

Fig. 8. Residual overlay with Mount Endut geological map

3.5. First Horizontal Derivative (FHD) Map

Based on the fault analysis on the residual-anomaly map, several faults are visible; however, the FHD method can be used to see a more apparent fault structure (Fig. 9). On the obtained FHD map, it can be assumed that there was a fault structure in the study area where the gravity anomaly distribution values ranged from 0.0007431 to 0.0107059 mGal. The FHD values with high anomalies (ranging from 0.0054794 to 0.0107059) were associated with the faults. The faults that trended north to south in the southern part of the study area are not visible on the residual map but can be clearly seen in the FHD map.

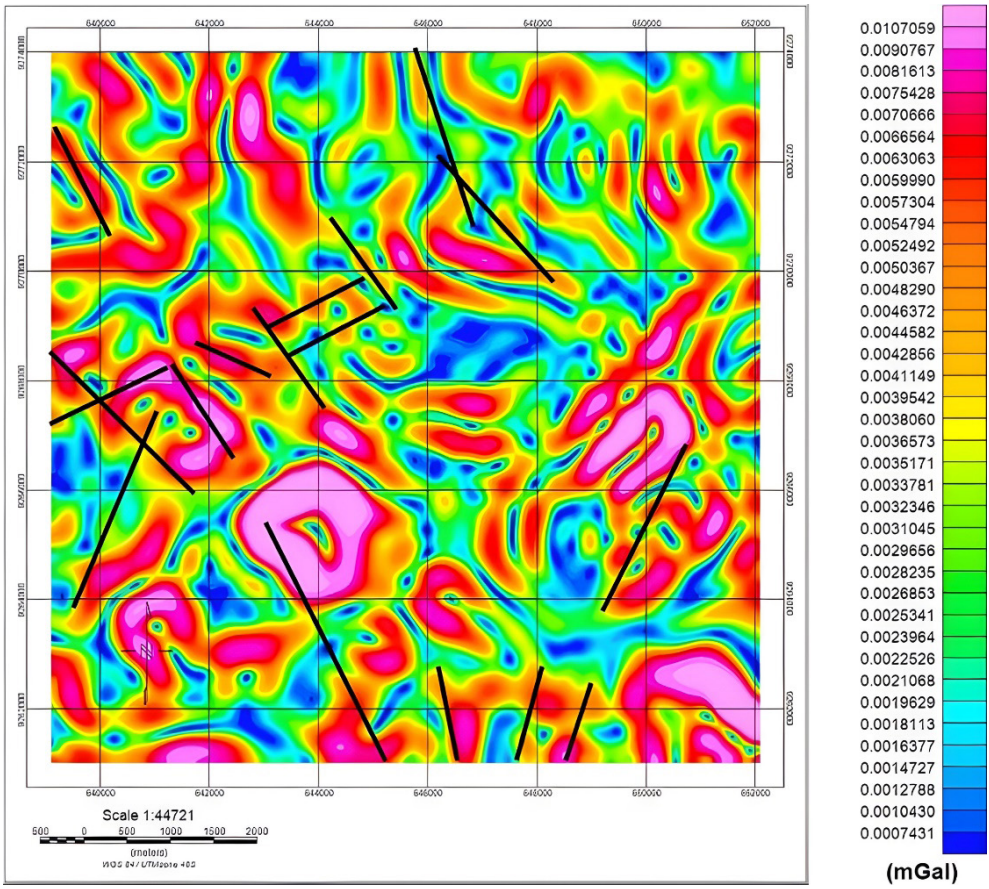

Fig. 9. FHD map

When analyzing the fault structure, however, the FHD information alone was not enough; for this reason, it needed to be supported by examining the SVD map.

3.6. Second Vertical Derivative (SVD) Map

The obtained SVD map had gravity-anomaly-distribution values that ranged from −0.0000393 to 0.0000339 mGal. On the SVD map (Fig. 10), the suspected faults were between the highest and lowest anomaly values (ranging from −0.000011 to 0.0000033 mGal). Based on the fault in the residual and FHD, these can be seen on the SVD map – namely, in diagonal directions (northwest-southeast and north-east-southwest) and a vertical direction (north-south). All of the faults on the SVD and FHD maps matched the faults that could be found in the geological map.

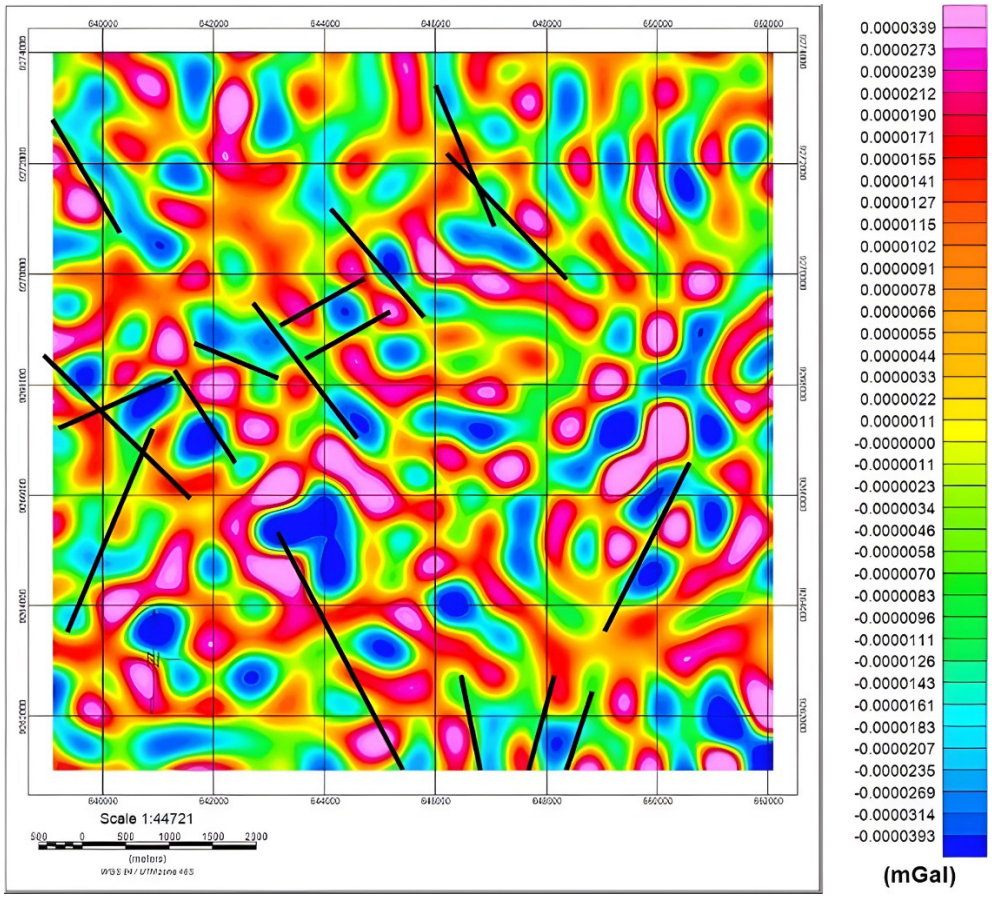

Fig. 10. SVD map

3.7. Fault Analysis

By ensuring that there are faults that control the geothermal manifestations in the study area, digitization was performed on as many as two tracks (Lines 1 and 2) on the residual map that were perpendicular to the direction of the faults (Fig. 11) and correlated with the geological data; this was where the anomaly was indicated as the fault structure that controlled the Cikawah and Handeuleum geothermal systems.

The presence of a fault indication on the digitized FHD in Figure 12 was indicated by an FHD value that had a maximum or peak value, while on SVD, the presence of a fault was indicated by an SVD value that was close to or equal to zero. The digitization path was made to intersect or be perpendicular to the direction of the fault, so that the fracture could be detected.

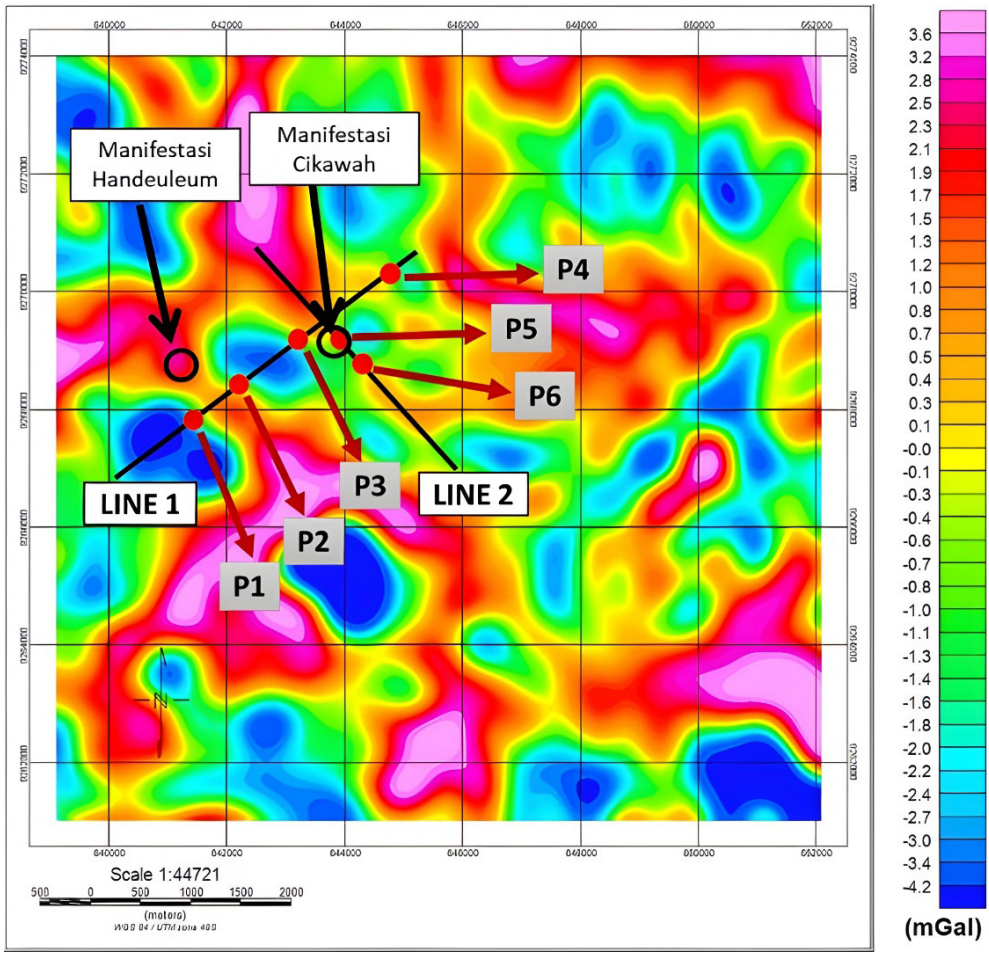

Fig. 11. Plot of fault points on residual anomaly map

The digitization results in Line 1 that led to the FHD and SVD graphs (Fig. 13) obtained four faults (marked P1, P2, P3, and P4). The P1 fault was a fault structure that trended northwest to southeast, which was at coordinates UTM (X) 641436.5 and UTM (Y) 9267766.6 (with an FHD peak value of 0.91 mGal and an SVD point value of 0.10 mGal). The P1 fault was a normal fault that was characterized by an absolute minimum SVD value that was smaller than the maximum SVD value. The P2 fault (Fig. 14) was a fault structure that trended northwest to southeast at coordinates UTM (X) of 642383.8 and UTM (Y) of 9268436.2, with a peak FHD value of 0.85 mGal and a minimum SVD-point value of 0.00 mGal. The P2 fault was suspected to be a horizontal fault; this was evidenced by the absolute minimum SVD value that was equal to the maximum SVD value.

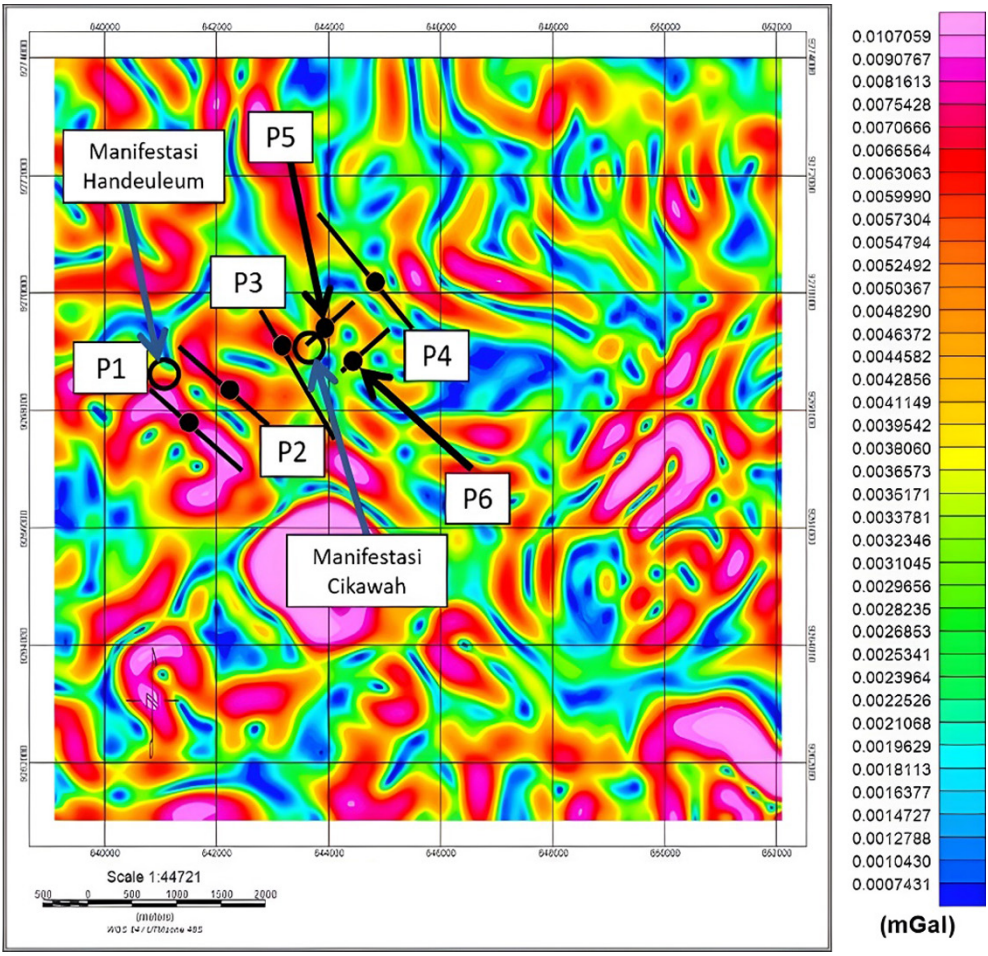

Fig. 12. Plot of fault points on FHD map

The P3 fault was a fault structure that trended northwest to southeast at coordinates UTM (X) of 643298.4 and UTM (Y) of 9269082.7, with a peak FHD value of 0.77 mGal and a minimum SVD-point value of 0.00 mGal. The P3 fault was normal, as was evidenced by the absolute minimum SVD value that was less than the maximum SVD. The P4 fault was a fault structure that trended northwest to southeast at coordinates UTM (X) of 644784.6 and UTM (Y) of 9270133.2, with a peak FHD value of 0.55 mGal and an SVD point value of 0.00 mGal. The P4 fault was suspected to be a thrust fault, which was evidenced by an absolute minimum SVD value that was greater than the maximum SVD. The analysis results of the four faults were by the geological conditions of the study area, where the P2 fault was a horizontal fault that was the path for the emergence of the Handeleum hot springs.

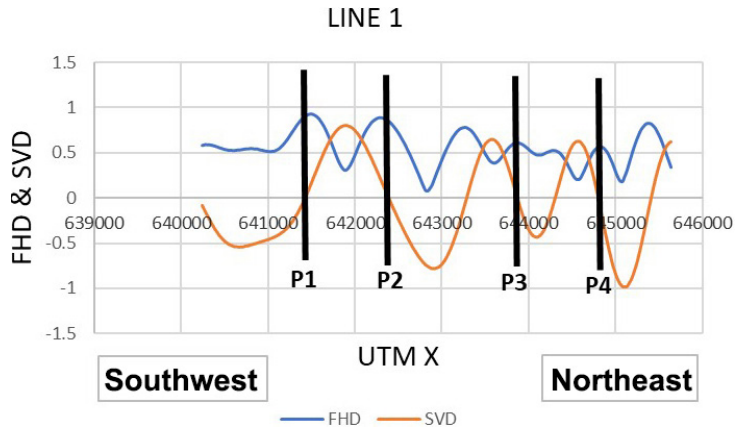

Fig. 13. FHD and SVD graphs on Line 1

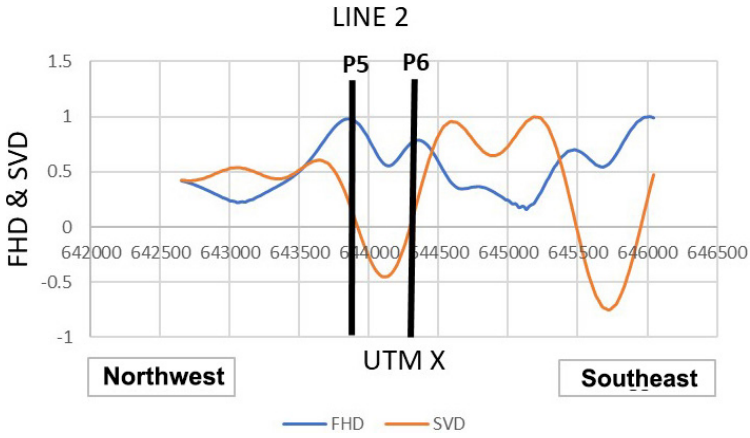

Fig. 14. FHD and SVD graphs on Line 2

The results of the digitization in Line 2 (Fig. 14) that produced the FHD and SVD graphs (Fig. 14) obtained two faults (P5 and P6). The P5 fault was a fault structure that trended northeast to southwest at coordinates UTM (X) 643906.2 and UTM (Y) 9269268.5, with a peak FHD value of 0.95 mGal and a minimum value of SVD point of 0.00 mGal. The P5 fault was a normal fault, as was evidenced by the absolute minimum SVD value that was less than the maximum SVD. The P6 fault was a fault structure that trended northeast to southwest at coordinates UTM (X) of 644309.8 and UTM (Y) of 9268824.5, with a peak FHD value of 0.76 mGal and a minimum value of SVD point of 0.00 mGal. The two faults followed the geological conditions of the study area, where the P6 fault was a normal fault that was the path for the emergence of the Cikawah hot springs.

3.8. 3D-Inversion Modeling

Based on the 3D modeling (Fig. 15) in the Cikawah and Handeleum hot springs areas, it could be seen that the structure was below the surface; namely, there was a fault in the northeast-to-southwest direction (red line) as the exit route for the Cikawah hot springs and another that trended northwest to southeast (black line) as the exit line of the Handelum hot springs. From the 3D results, it could be seen that there was a layer of blue-green color under the Cikawah and Handeleum hot springs; this was a cap rock with a rock density of 2.52–2.58 g/cm^3, which was suspected to be clay rock with depths that ranged from 0 to 1250 m. The white-to-yellow layers were reservoir rocks with densities of 2.60–2.66 g/cm^3; these were suspected to be lava rocks that were weathered due to the hydrothermal flows and mixed meteoric water, with depths that ranged from 1500 to 3000 m. The red layer was a heat source that was suspected to be an igneous intrusion that was below the surface of the Cikawah manifestation, with density values of 2.70–2.72 g/cm^3 at depths that ranged from 1750 to 3000 m.

The heat-source layer (which is shown in red under the surface of the Cikawah and Handeleum manifestations) originated from one source; namely, in the eastern part of Mount Endut, which is thought to be an intrusion of a frozen relief that was produced by Mount Endut. So, it can be said that the manifestation areas of Cikawah and Handeleum are included in one geothermal system, with the distance between the manifestations of Cikawah and Handeleum around 2500 m.

Comparing this gravity method with another geophysics method in the geothermal field, the document entitled "Geoscientific Studies of Geothermal Resources of Gunung Endut Area, Banten Province, West Jawa-Indonesia" by Alanda Idral et al. [47] presented a comprehensive assessment of the geothermal potential in the Mount Endut area through integrated geoscientific methods. The study utilized geological mapping to identify the rock types and formations along with a petrographic analysis and K/Ar dating for the age determination. The geochemical analyses involved collecting hot water and gas samples for laboratory testing, which employed geothermometers (SiO_2 and Na-K) to estimate the subsurface temperatures based on the surface-water chemistry. Additionally, the geophysical surveys included gravity measurements from 247 observation points and DC resistivity surveys at various depths for analyzing the subsurface structures. The results revealed that the surface hot-water temperatures ranged from 53 to 88°C, with neutral pH levels, while estimated subsurface temperatures that were calculated using geothermometry were between 162 and 180°C, thus indicating an intermediate enthalpy geothermal system. The geological findings highlighted volcanic rocks that were associated with the Quaternary volcanism in the region, which was characterized by normal faults that controlled fluid movement toward surface manifestations (like the Cikawah and Handeuleum hot springs). The gravity data indicated high-density contrasts, which suggested possible intrusive bodies beneath these areas that were related to geothermal activity.

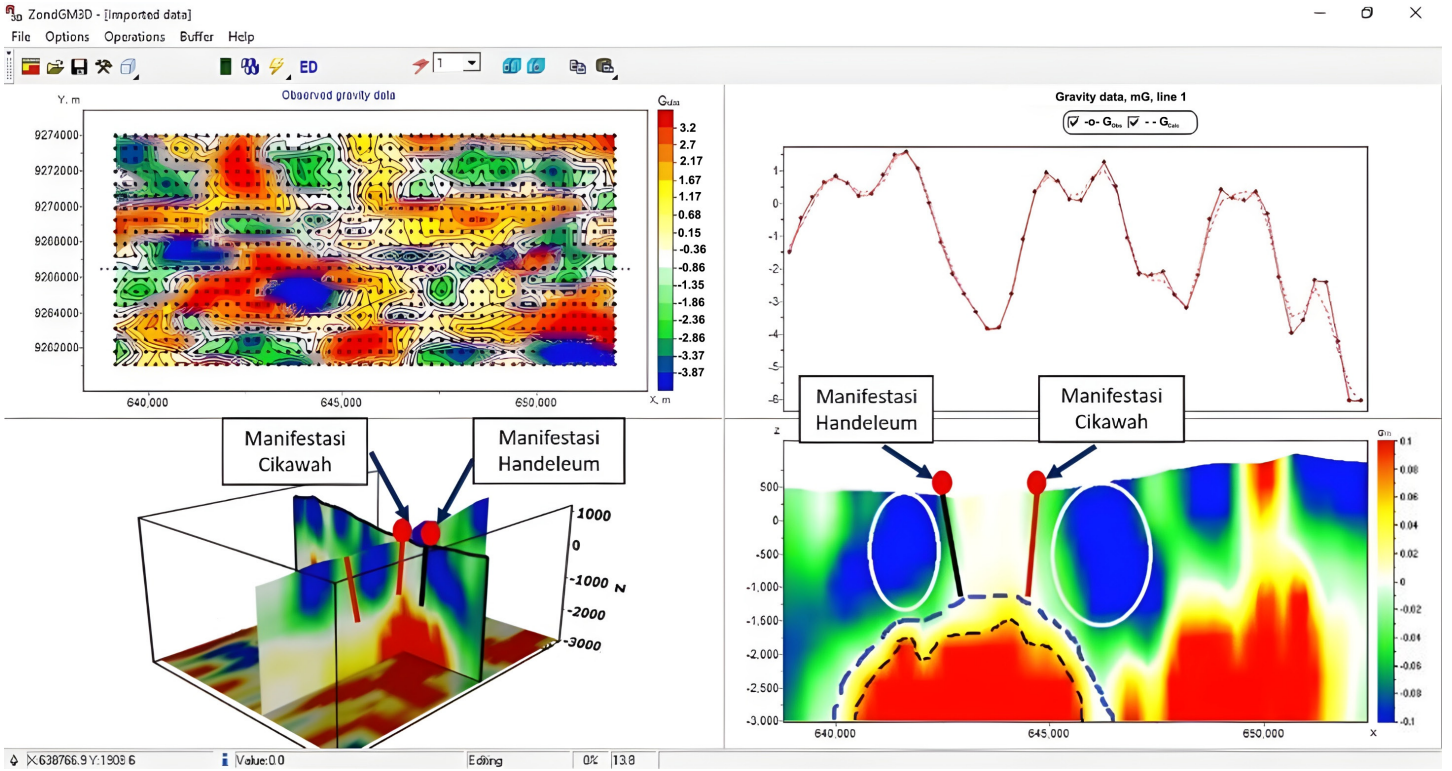

Fig. 15. 3D modeling in Cikawah and Handeleum areas

The resistivity data showed low resistivity zones that were linked to altered rocks at depths that were greater than 1000 m; these likely corresponded to geothermal reservoirs where fluids accumulated due to tectonic processes. The hydrogeological assessment classified areas into recharge zones (where meteoric water infiltrated), discharge zones (where groundwater emerged), and runoff waters that contributed less directly to the thermal systems. The prospect area covered approximately 4.5 km^2, with an estimated energy potential of 60 MWe. The study concluded that a concealed stock-like intrusive body was suggested as a heat source due to its association with the volcanic activity in the region; it recommended further explorations through magnetotelluric (MT) methods, followed by drilling at identified sites for more-accurate assessments before development could proceed effectively. The figures that were presented in this document contained valuable data that was pertinent to the geothermal analysis; however, they generally lacked clarity and sufficient context for an effective interpretation. Many figures did not provide clear labels nor legends that would help elucidate the significance of the data points or trends that were depicted.

Utilizing GGMplus data for the gravity modeling presented a cost-effective approach as compared to conducting a full integration of geoscientific methods for our preliminary research. One of the primary advantages was the free access to GGMplus, which provided global gravity-field models that were derived from satellite data, thus eliminating the need for the expensive field surveys and equipment that are typically required for local gravity measurements. This significantly reduced the costs that are associated with mobilizing teams, transportation, and logistics that come with extensive ground-based measurements. Additionally, the rapid availability of pre-existing GGMplus data allowed the researchers to quickly access and analyze gravity information without any delays that are related to planning new field campaigns, thereby expediting the preliminary assessments. For many initial investigations – especially in large or remote areas where detailed local surveys may not be feasible – GGMplus offers sufficient spatial resolution for identifying broad geological features and anomalies that are indicative of subsurface structures. This enables researchers to gain insights into regional trends in gravitational anomalies that could guide further investigation without incurring high upfront costs. Furthermore, GGMplus can be used complementarily with other data sets (e.g., magnetic or seismic) at a minimal additional expense while reserving comprehensive integrated approaches for later stages when specific targets are identified. Starting with inexpensive GGMplus data also allows researchers to scale their studies progressively; if significant anomalies are detected that warrant further investigation, funds can then be allocated toward more-intensive geoscientific methods such as localized gravity surveys or drilling. Ultimately, employing GGMplus as a basis for gravity modeling optimizes resource allocation by enabling focused funding on high-potential areas that are identified through preliminary analyses rather than prematurely spreading resources thinly across extensive full-scale studies. In summary, leveraging GGMplus data provides an efficient means for gathering essential insights during

early geothermal research stages while minimizing costs and facilitating informed decision-making regarding subsequent investigative efforts based on initial findings.

We recognize that the findings from this study of Mount Endut can significantly contribute to the broader field of geothermal research and exploration. The geological and geophysical insights that were gained from this investigation not only enhance our understanding of the geothermal potential at Mount Endut but also provide valuable lessons that are applicable to other regions with similar geological characteristics.

First, the successful application of advanced geophysical methods such as gravity-anomaly analysis and 3D-inversion modeling demonstrates the effectiveness of these techniques in identifying geothermal resources in complex geological settings; those regions with similar tectonic and volcanic histories – particularly those that are characterized by fault systems and varied rock types – can benefit from adopting these methodologies. As was employed in our study, the integration of multiple geophysical techniques can lead to more-accurate assessments of geothermal potential, thereby improving exploration strategies in analogous areas.

Moreover, our findings regarding the relationship between geological structures such as faults and geothermal manifestations highlight the importance of detailed geological mapping and structural analysis in geothermal exploration. Understanding how fault systems influence the movements of geothermal fluids and the locations of hot springs can guide exploration efforts in other regions [48]. This knowledge can help identify prospective areas for drilling and resource development, ultimately leading to more-efficient and targeted exploration campaigns.

Additionally, the implications of our study extend to the environmental and economic aspects of geothermal energy development. By demonstrating the viability of geothermal resources in a specific geological context, our research can encourage investment and interest in geothermal exploration in similar regions. This is particularly relevant in the context of global efforts to transition to renewable energy sources, where geothermal energy presents a sustainable option for meeting energy demands while minimizing environmental impacts.

The investigation of the geothermal prospects at Mount Endut offers significant implications for geothermal exploration under comparable geological conditions. The methodologies and insights that were derived from this study can serve as a valuable reference for future research and exploration efforts in regions with similar geological features, ultimately contributing to the sustainable development of geothermal energy resources worldwide. We appreciate the reviewers' emphasis on this aspect, as it highlights the broader relevance of our findings in the context of geothermal exploration and resource management.

4. Conclusion

The analyses of FHD and SVD revealed six distinct geological structures in Mount Endut, with two faults that influenced the manifestation of the Handeleum

hot springs. These faults are aligned along a northwest-to-southeast trend and consist of one normal fault and one horizontal fault. The horizontal fault is considered to be the path for the emergence of the Handeleum hot springs. Meanwhile, four faults control the manifestation of Cikawah, with two faults trending northwest to southeast (which are normal and rising faults) and two faults trending southwest to northeast (which are normal fault types) as a pathway for the emergence of the Cikawah hot springs.

The 3D-inversion modeling results further indicated that the Handeleum and Cikawah manifestation areas were underlain by cover layers with densities that ranged from 2.52 to 2.58 g/cm^3, which are suspected to be clay at average depths that range between 0 and 1250 m. With densities ranging from 2.60 to 2.66 g/cm^3, the reservoir layer was suspected to be lava rock at average depths that ranged from 1500 to 3000 m, and the heat-source layer that had densities that ranged from 2.70 to 2.72 g/cm^3 was suspected to be an igneous intrusion at average depth of 1750–3000 m. These findings suggested that both the Handeleum and Cikawah manifestations were part of a geothermal system that originated from the geothermal production beneath Mount Endut.

Funding

This research received no specific grant from any funding agency in the public, commercial, or not-for-profit sectors.

CRediT Author Contribution

H. S.: conceptualization, experiment methodology, data curation, original draft preparation, review and editing, project administration, supervision.

B. P.: conceptualization, experiment methodology, data curation, original draft preparation, review and editing, project administration, supervision.

A. R.: conceptualization, experiment methodology, data curation, original draft preparation, review and editing, project administration, supervision.

A. A. M.: conceptualization, experiment methodology, software, validation, review, and editing.

T. A. P. S.: conceptualization, experiment methodology, software, validation, review, and editing.

N. H.: conceptualization, experiment methodology, software, validation, review, and editing.

A. F. R.: conceptualization, experiment methodology, formal analysis, investigation, review, and editing.

Y. S.: conceptualization, experiment methodology, formal analysis, investigation, review, and editing.

T.: conceptualization, experiment methodology, formal analysis, investigation, review, and editing.

B. S.: conceptualization, experiment methodology, formal analysis, investigation, review, and editing.

Declaration of Competing Interests

The authors declare that they have no known competing financial interests or personal relationships that could have appeared to influence the work that is reported in this paper.

Data Availability

The data that support the findings of this study are openly available via the following links:

http://ddfe.curtin.edu.au/models/GGMplus/

https://ddfe.blazejbucha.com/models/GGMplus/

References

[1] Sobirin R., Permadi A.N., Akbar A.M., Wildan D., Supriyanto: *Analysis geothermal prospect of Mt. Endut using geochemistry methods*. AIP Conference Proceedings, vol. 1862(1), 2017, 030187. https://doi.org/10.1063/1.4991291.

[2] Supriyanto, Maryadi Maryadi, Sahdarani D.N., Zarkasyi A.: *Geoelectrical methods for geothermal exploration in Endut geothermal prospect area, Banten Province, Indonesia*. International Journal of GEOMATE, vol. 17(63), 2019, pp. 241–248. https://doi.org/10.21660/2019.63.98151.

[3] Tanjung F.H., Dhianaufal, Rahmadhani A.U., Sihombing F.M.H., Sahdarani D.N., Supriyanto: *Lineament mapping using remote sensing and correlation on surface manifestation distribution in Gunung Endut, Banten Province, Indonesia*. IOP Conference Series: Earth and Environmental Science, vol. 538(1), 2020, 012051. https://doi.org/10.1088/1755-1315/538/1/012051.

[4] Maryadi M., Cahyanto T., Nugraha A.D., Riyanto A., Kusdaryanto T., Suryantini, Supriyanto: *Geoelectrical methods for geothermal exploration in Endut geothermal prospect area, Banten Province, Indonesia*. International Journal of GEOMATE, vol. 17(63), 2019, pp. 241–248. https://doi.org/10.21660/2019.63.98151.

[5] Akbar A.M., Permadi A.N., Wildan D., Sobirin R., Supriyanto: *Application of remote sensing analysis and MT method for identification geothermal prospect zone in Mt. Endut*. AIP Conference Proceedings, vol. 1862(1), 2017, 030183. https://doi.org/10.1063/1.4991287.

[6] Supriyanto, Noor T., Suhanto E.: *Analysis of gravity data beneath Endut geothermal prospect using horizontal gradient and Euler deconvolution*. AIP Conference Proceedings, vol. 1862(1), 2017, 030194 . https://doi.org/10.1063/1.4991298.

[7] Hirt C., Claessens S., Fecher T., Kuhn M., Pail R., Rexer M.: *New ultra-high resolution picture of Earth's gravity field*. Geophysical Research Letters, vol. 39(2), 2012, pp. 4279–4283. https://doi.org/10.1002/grl.50838.

[8] Suprianto A., Supriyadi, Priyantari N., Cahyono B.E.: *Correlation between GGMPlus, TOPEX and BGI gravity data in volcanic areas of Java Island*. Journal of Physics: Conference Series, vol. 1825(1), 2021, 012023. https://doi.org/10.1088/1742-6596/1825/1/012023.

[9] Hirt C., Kuhn M., Claessens S., Pail R., Seitz K., Gruber T.: *Study of the Earth's short-scale gravity field using the ERTM2160 gravity model*. Computers & Geosciences, vol. 73, 2014, pp. 71–80. https://doi.org/10.1016/j.cageo.2014.09.001.

[10] Liu J.: *Using gravity gradient component and their combination to interpret the geological structures in the eastern Tianshan Mountains*. Geophysical Journal International, vol. 228(2), 2022, pp. 982–998. https://doi.org/10.1093/gji/ggab373.

[11] Setyawan A., Khusna L.M., Suseno J.E., Rina D.I., Yulianto T., Aribowo Y.: *Detecting hot spring manifestations based on gravity data satellite on mountain Lawu*. Journal of Physics: Conference Series, vol. 1943(1), 2021, 012034. https://doi.org/10.1088/1742-6596/1943/1/012034.

[12] Yanis M., Abdullah F., Zaini N., Ismail N.: *The northernmost part of the Great Sumatran Fault map and images derived from gravity anomaly*. Acta Geophysica, vol. 69(3), 2021, pp. 795–807. https://doi.org/10.1007/s11600-021-00567-9.

[13] Lambeva T.: *Estimation of normal and geopotential height differences derived by gravity data from global geopotential models for the territory of Bulgaria*, [in:] Rivza B., Trofymchuk O. (eds.), *21st International Multidisciplinary Scientific GeoConference SGEM 2021*, vol. 21(2.1), STEF92 Technology, Sofia 2021, pp. 155–166. https://doi.org/10.5593/sgem2021/2.1/s09.45.

[14] Aziz K.N., Hartantyo E., Niasari S.W.: *The study of fault lineament pattern of the Lamongan Volcanic Field using gravity data*. Journal of Physics: Conference Series, vol. 1011(1), 2018, 012025. https://doi.org/10.1088/1742-6596/1011/1/012025.

[15] Juwita W., Permadi A.N., Akbar A.M., Wildan D., Supriyanto: *Identification of potential hydrocarbon traps using the gravity method in the Bengkulu basin*. Iranian Journal of Geophysics, vol. 18(3), 2024, pp. 69–83. https://doi.org/10.30499/ijg.2023.409882.1535.

[16] Hudayat N., Rahman S.A.N., Martha A.A., Sutrisno S., Wulandari A.: *Identification of subsurface structures and potential reservoir zones of geothermal fields based on gravity data analysis in the Karaha-Cakrabuana area, West Java*. Iranian Journal of Geophysics, 2024 [in press]. https://doi.org/10.30499/ijg.2024.434652.1563.

[17] Rosid M.S., Siregar H.: *Determining fault structure using first horizontal derivative (FHD) and horizontal vertical diagonal maxima (HVDM) method: A comparative study*. AIP Conference Proceedings, vol. 1862(1), 2017, 030171. https://doi.org/10.1063/1.4991275.

[18] Supriyadi, Soraya V., Suprianto A., Priyantari N.: *Identification of Blawan-Ijen fault based on GGMplus gravity data using second vertical derivative (SVD) analysis*. AIP Conference Proceedings, vol. 2663(1), 2022, 040005. https://doi.org/10.1063/5.0108055.

[19] Supriyanto, Rokhmatuloh, Sobirin R., Suhanto E.: *The effect of gravity measurement distribution points on interpretation of gravity data in the Gunung Endut geothermal prospect area, Indonesia*. International Journal of GEOMATE, vol. 14(41), 2018, pp. 60–67. https://doi.org/10.21660/2018.41.07022.

[20] Thanh Pham L., Eldosouky A.M., Melouah O., Abdelrahman K., Alzahrani H., Oliveira S.P., Andráš P.: *Mapping subsurface structural lineaments using the edge filters of gravity data*. Journal of King Saud University – Science, vol. 33(8), 2021, 101594. https://doi.org/10.1016/j.jksus.2021.101594.

[21] Kusnadi D., Idral A., Rezky Y., Suhanto E., Sumardi E.: *Penyelidikan terpadu panas bumi daerah Gunung Endut, Kabupaten Lebak, Banten*, [in:] *Proceeding Pemaparan Hasil-Hasil Kegiatan Lapangan dan Non Lapangan Tahun 2006*, Pusat Sumber Daya Geologi, Bandung 2006, pp. 1–14.

[22] Pramadhani F., Rokhmatulloh, Supriatna: *Potensi panas bumi berdasarkan karakteristik fisik wilayah (Studi Kasus: Daerah Wayang-Windu, Kabupaten Bandung, Propinsi Jawa Barat dan Daerah Gunung Endut, Kabupaten Lebak, Propinsi Banten)*. Jurnal Geosains Terapan, vol. 1(1), 2015, pp. 18–28. https://geosainsterapan.id/index.php/id/article/view/4.

[23] Widodo S., Kusnadi D., Kholid M., Rezky Y.: *Evaluasi potensi panas bumi daerah Gunung Endut Kabupaten Lebak – Provinsi Banten*, [in:] *Prosiding Hasil Kegiatan Lapangan Pusat Sumber Daya Geologi Tahun Anggaran 2009: Bidang Mineral*, Pusat Sumber Daya Geologi, Bandung 2010, pp. 357–367.

[24] Atkinson N.: *GOCE Satellite Begins Mapping Earth's Gravity in Lower Orbit Than Expected*. *Universe Today*, September 30, 2009. https://www.universetoday.com/41821/goce-satellite-begins-mapping-earths-gravity-in-lower-orbit-than-expected/ [access: 23.06.2021].

[25] Hirt C.: *RTM gravity forward-modeling using topography/bathymetry data to improve high-degree global geopotential models in the coastal zone*. Marine Geodesy, vol. 36(2), 2013, pp. 183–202. https://doi.org/10.1080/01490419.2013.779334.

[26] Rexer M., Hirt C., Bucha B., Holmes S.: *Solution to the spectral filter problem of residual terrain modelling (RTM)*. Journal of Geodesy, vol. 92(6), 2018, pp. 675–690. https://doi.org/10.1007/s00190-017-1086-y.

[27] Yasmin H.S., Setiawan T., Kusuma R., Ramadhan D., Nugraha F.: *2D geological structure identification in Mount Ciremai geothermal area using the GGMplus data*. IOP Conference Series: Earth and Environmental Science, vol. 1344(1), 2024, 012017. https://doi.org/10.1088/1755-1315/1344/1/012017.

[28] Alqahtani F., Ehsan M., Aboud E., Abdulfarraj M., El-Masry N.: *Integrated approach using petrophysical, gravity, and magnetic data to evaluate the geothermal resources at the Rahat Volcanic Field, Saudi Arabia*. Frontiers in Earth Science, vol. 11, pp. 1–16, 2023. https://doi.org/10.3389/feart.2023.1135635.

[29] Liu Q., Schmidt M., Sánchez L.: *Combination of different observation types through a multi-resolution representation of the regional gravity field using the*

pyramid algorithm and parameter estimation. Journal of Geodesy, vol. 96(10), pp. 1–20, 2022. https://doi.org/10.1007/s00190-022-01670-5.

[30] Umar E.P., Harijoko A., Setianto A., Suryanto W.: *Structural map of Sulawesi derives from gravity data and its implications for geothermal systems*. E3S Web of Conferences, vol. 468, 2023, 4004. https://doi.org/10.1051/e3sconf/202346804004.

[31] Apeh O.I., Tenzer R.: *Selection of an optimum global gravitational model for geological mapping of Afikpo and Anambra Basins in Nigeria*. Geodesy and Cartography, vol. 48(2), pp. 92–106, 2022. https://doi.org/10.3846/gac.2022.14551.

[32] Lemenkova P.: *GRASS GIS for topographic and geophysical mapping of the Peru-Chile Trench*. Forum Geograficum, vol. 19(2), 2020, pp. 143–157. https://doi.org/10.5775/fg.2020.009.d.

[33] Sehah, Prabowo U.N., Raharjo S.A., Ikhwana A.Z.: *Physical modeling of magma chamber of Slamet volcano by means of satellite gravimetric data*. Communications in Science and Technology, vol. 7(2), 2022, pp. 160–167. https://doi.org/10.21924/cst.7.2.2022.1001.

[34] Ikhwandi A.F.F.P.F.L., Hadi A.I., Zakariya H., Refrizon R.: *Identification of the Manna Segment Sumatran Fault using GGMplus gravity anomaly data with the second vertical derivative (SVD) method*. Jurnal Ilmu Fisika Universitas Andalas, vol. 15(2), 2023, pp. 123–136. https://doi.org/10.25077/jif.15.2.123-136.2023.

[35] Putra U.G., Jhanesta W., Iskandarsyah: *Interpretation of subsurface fault through multi-level second vertical derivative gravitational data in Bittuang Geothermal Working Area, South Sulawesi, Indonesia*. Journal of Geoscience, Engineering, Environment, and Technology, vol. 6(4), 2021, pp. 184–191. https://doi.org/10.25299/jgeet.2021.6.4.7744.

[36] Legowo B., Nailatunisrina R., Purwanto H., Purnama B., Suryanto W.: *Modelling of Volcano Lawu fault structure using gravity anomaly to determine landslides potential*. IOP Conference Series: Earth and Environmental Science, vol. 986(1), 2022, 012025. https://doi.org/10.1088/1755-1315/986/1/012025.

[37] Reynolds J.M.: *An Introduction to Applied and Environmental Geophysics*. 2nd ed., John Wiley & Sons, Chichester 2011.

[38] Telford W.M., Geldart L.P., Sheriff R.E.: *Applied Geophysics*. 2nd ed. Cambridge University Press, Cambridge 1990.

[39] Akhadi M., Harahap D., Subakti H., Wandono: *The utilization of GGMplus data using derivative method and 3D modeling of subsurface structure for Trienggadeng Fault identification in Pidie Jaya, Aceh Region*. Journal of Physics: Conference Series, vol. 1805(1), 2021, 012037. https://doi.org/10.1088/1742-6596/1805/1/012037.

[40] Saada S.A., Eleraki M., Mansour A., Eldosouky A.M.: *Insights on the structural framework of the Egyptian Eastern Desert derived from edge detectors of gravity data*. Interpretation, vol. 13(1), 20252024, pp. 1–40. https://doi.org/10.1190/int-2024-0023.1.

[41] Camacho M., Alvarez R.: *Geophysical modeling with satellite gravity data: Eigen-6C4 vs. GGMplus*. Engineering, vol. 13(12), 2021, pp. 690–706. https://doi.org/10.4236/eng.2021.1312050.

[42] Hidayat L.N., Syafrudin T.R., Suwesti A., Khakim U.A., Astuti M.D., Hanafi M.I.: *Bandpass filter untuk data seismic*, [in:] Abdullah W.A., Heriyanto M., Prabusetyo H.R. (eds.), *Komputasi Geofisika 1: Pemodelan dan Prosesing Geofisika dengan Octave/Matlab*, Program Studi Teknik Geofisika, Fakultas Teknologi Eksplorasi dan Produksi, Jakarta 2018, pp. 17–26. https://doi.org/10.6084/m9.figshare.5946688.

[43] Kearey P.: *An Introduction to Geophysical Exploration*. 3rd ed., Blackwell Publishing, Oxford 2002.

[44] Sarkowi M., Wibowo R.C.: *Geothermal reservoir identification based on gravity data analysis in Rajabasa Area – Lampung*. Riset Geologi dan Pertambangan – Indonesian Journal of Geology and Mining, vol. 31(2), 2021, pp. 77–97. https://doi.org/10.14203/risetgeotam2021.v31.1164.

[45] Grandis H.: *Pengantar Pemodelan Inversi Geofisika*. Himpunan Ahli Geofisika Indonesia (HAGI), Jakarta 2009. https://doi.org/10.17605/OSF.IO/PHGCW.

[46] Jhanesta W., Supriyanto: *Application of Multi-Level Second Vertical Derivative (ML-SVD) method to identify subsurface structure in Mount Endut geothermal prospect area, Indonesia*, [in:] *Proceedings of the 2nd Digital Indonesia International Geothermal Convention (DIIGC)*, Indonesian Geothermal Association (INAGA), Jakarta 2021, pp. 1–7. https://www.researchgate.net/publication/358571529.

[47] Idral A., Rezky Y., Kusnadi D., Sumardi E., Mustang A.: *Geoscientific studies of geothermal resources of Gunung Endut Area, Banten Province – West Jawa, Indones*ia, [in:] *48th Workshop on Geothermal Reservoir Engineering, Stanford, California, 6–8 February 2023*, SGP-TR-224, Stanford Geothermal Program, Stanford 2024, pp. 195–209.

[48] Melouah O., Ebong E.D., Abdelrahman K., Eldosouky A.M.: *Lithospheric structural dynamics and geothermal modeling of the Western Arabian Shield*. Scientific Reports, vol. 13(1), 2023, pp. 1–30. https://doi.org/10.1038/s41598-023-38321-4.